

Evaluating Effects of Shear Processing on 2D Crystalline Materials in 3D Metal Matrices

Atomistic Understanding of High Shear Deformation of Copper Graphene Composites

September 2021

Bharat Gwalani
Mayur Pole
Kate Whalen
Shuang Li
Brian O'Callahan
Jinhui Tao
Aditya Nittala
Keerti Kappagantula

DISCLAIMER

This report was prepared as an account of work sponsored by an agency of the United States Government. Neither the United States Government nor any agency thereof, nor Battelle Memorial Institute, nor any of their employees, **makes any warranty, express or implied, or assumes any legal liability or responsibility for the accuracy, completeness, or usefulness of any information, apparatus, product, or process disclosed, or represents that its use would not infringe privately owned rights.** Reference herein to any specific commercial product, process, or service by trade name, trademark, manufacturer, or otherwise does not necessarily constitute or imply its endorsement, recommendation, or favoring by the United States Government or any agency thereof, or Battelle Memorial Institute. The views and opinions of authors expressed herein do not necessarily state or reflect those of the United States Government or any agency thereof.

PACIFIC NORTHWEST NATIONAL LABORATORY
operated by
BATTELLE
for the
UNITED STATES DEPARTMENT OF ENERGY
under Contract DE-AC05-76RL01830

Printed in the United States of America

Available to DOE and DOE contractors from
the Office of Scientific and Technical
Information,
P.O. Box 62, Oak Ridge, TN 37831-0062
www.osti.gov
ph: (865) 576-8401
fox: (865) 576-5728
email: reports@osti.gov

Available to the public from the National Technical Information Service
5301 Shawnee Rd., Alexandria, VA 22312
ph: (800) 553-NTIS (6847)
or (703) 605-6000
email: info@ntis.gov
Online ordering: <http://www.ntis.gov>

Evaluating Effects of Shear Processing on 2D Crystalline Materials in 3D Metal Matrices

Atomistic Understanding of High Shear Deformation of Copper Graphene Composites

September 2021

Bharat Gwalani
Mayur Pole
Kate Whalen
Shuang Li
Brian O'Callahan
Jinhui Tao
Aditya Nittala
Keerti Kappagantula

Prepared for
the U.S. Department of Energy
under Contract DE-AC05-76RL01830

Pacific Northwest National Laboratory
Richland, Washington 99354

Table of Contents

Executive Summary	3
1.0 Introduction.....	4
2.0 Materials and Methods	6
2.1 Materials	6
2.2 Shear Processing and Microstructural Characterization.....	6
3.0 Results & Discussion.....	7
3.1 Tribological Behavior of Cu-Gr Composites	7
3.2 Composition of Sheared Cu-Gr Composites	9
3.3 Nanostructures in Shear Processed Cu-Gr Composites.....	10
4.0 Conclusions.....	13
References	14

Executive Summary

Composites made of copper and graphene demonstrate high strength, lubricity and enhanced electrical and thermal conductivity compared pure copper. However, manufacturing these composites at bulk volumes for industrial applications has been a big challenge. Shear deformation assisted processing is an effective method for manufacturing materials such as copper-graphene composites demonstrating ultra-fine grain structures and compositional homogeneity. Nevertheless, microstructural evolution of the composites and their property development under such conditions is not clearly understood currently. To rectify this gap in literature, high strain shear deformation of copper coated graphene foils was performed using a tribometer pin in this study. Changes in microstructure of the composite as well as the constituent components under shear deformation was correlated to process conditions. A sharp increase in the coefficient of friction attributed to rupture and smearing of graphene layer into copper substrate was observed during the shear processing. The coefficient of friction of the sheared copper/graphene composite was lower than that of pure copper, suggesting that partially worn graphene is effectively lubricious at the macroscale. A multimodal characterization of the processed region further revealed a shear deformation-induced ultrafine two-phase grain-structure consisting of copper and graphitic domains. Shear deformation reduced the copper grain size from around 50 – 100 μm to ~ 200 nm on an average and ~ 2 – 5 nm in some locations. The semicrystalline graphene films were observed to fracture into 10 – 50 μm size flakes. Oxygen enrichment was observed in the processed region. Finally, graphitic domain were identified for the first time in the copper matrix and not just at the grain boundaries providing evidence for a metastable composite microstructure as a result of solid phase processing at room temperature.

1.0 Introduction

Copper (Cu)-graphene (Gr) composites have exceptional tribological, electrical, mechanical, and thermal properties, and have proved to be useful in several industrial applications such as sliding electrical contacts (1), high temperature conductors (2), and high strength bearings (3, 4). Despite numerous advantages of Cu-Gr composites over the conventional Cu alloys, their commercial applicability is limited due to a lack of manufacturing approaches that can manufacture bulk volumes while ensuring the development of optimal microstructural arrangement of the constituent components. Gr tends to agglomerate to reduce its surface energy thus making it difficult to uniformly disperse in a metal matrix (5). As Gr and Cu have no wettability and covalent bonding is also not possible as no reaction takes place between them until around 1000 °C, weak mechanical adhesion and van der Waals interaction are only viable approaches to developing a composite.

Solid phase processing approaches such as hot-extrusion (HE), shear assisted processing and extrusion (ShAPE™), superplastic deformation (SPD), friction extrusion (FE), friction stir processing (FSP), equichannel assisted processing/extrusion (ECAP/E), high pressure torsion (HPT), and hot-forging, where a final product is developed by processing materials at temperatures much lower than their melting points, have shown great promise in developing homogeneous composite microstructures. Of these, processes where high shear is applied, like HPT, ShAPE, ECAP/E, FE and SPD have shown that it is relatively easy to develop microstructures in Cu-Gr composites where the Gr is uniformly distributed through the Cu microstructures without agglomerations. In this context, the effects of shear processing on Cu and Cu alloys and their individual microstructural evolution is well documented in literature. On the other hand, there is limited exploration of the effects of shear/friction processing on Gr and the ensuing microstructure. Additionally, there is a gap in literature on understanding the microstructural evolution of a 2D material such as Gr in a 3D matrix such as Cu, especially at the macroscale. In particular, it is not clear if the 2D Gr transforms into 3D forms. Also not understood is the topology of the Gr in a metal matrix. Furthermore, in addition to distributing Gr in the Cu microstructure, high shear forces experienced by Cu-Gr during shear processing have also been correlated with the development of defects in Gr, which has a dramatic effect on the performance of composite. However, the process conditions that lead to this phenomenon are not well-understood currently.

Incidentally, most of the studies in literature describe the behavior of Gr ‘particles’ or ‘powders’ (that are 3D in nature) when processed alongside Cu and not 2D monolayer, atomically thin Gr. Technically, Gr powders and flakes are nanoscale graphite particles rather than Gr. As such, during shear processing, they have been shown to delaminate into Gr-like flakes and subsequently show enhanced defect densities. However, it is still not clear in literature how atomically thin Gr layer would deform or fracture under shear processing conditions.

To clearly elucidate the effects of thermomechanical process conditions experienced by Cu and Gr during shear processing of the Cu-Gr composite, it is essential to deform low defect density Gr in a Cu matrix under the same processing conditions as experienced during SPD, ShAPE or FE. In order to deconvolute complex thermomechanical processing conditions, experiments are performed where the material of interest is subjected to mechanical and thermal conditions progressively and the microstructural evolution is observed. Tribometer experiments provide a relatively easy pathway to applying shear forces (alone) in the absence of thermal effects to material systems in order to understand the sequential changes in microstructure albeit under the effects of mechanical processing alone. On the other hand, relevant temperature conditions

experienced by the materials during SPP are developed using electrical or thermal heating approaches such as resistance or inductive heaters, microwaves, lasers or furnaces. This study focuses on the application of mechanical stresses alone on Cu-Gr composites to study their structural evolution in the absence of thermal effects. It has to be noted that future work correlating shear forces at elevated temperatures to microstructural changes typically experienced by the materials during shear processing are also being explored but are not the focus of the present report.

Few tribometer experiments have been performed on Cu-Gr composites where the Gr was in the form of low defect density 2D monolayer films to evaluate the effects of process conditions on composite coefficient of friction (CoF) and graphene deformation/fracture post processing (3, 6, 7). In all these papers, it was seen that the Cu and Gr were strained under the action of tribometer pin. There is a critical load under which the CoF is very low for monolayer Gr films; beyond the threshold of critical load, wear of Gr layer gradually increases the CoF (7) which is hypothesized to be due to the formation of an amorphous carbon (C) layer on the wear track for wear experiments performed (8). The CoF of Gr flakes is also correlated to atomic vacancies in that higher defect density corresponds to higher CoF (10). In addition to experimental evaluation, first principles simulation work was also performed to understand the shear mechanism of Cu-Gr composites. Molecular dynamic (MD) simulations show two separate wear and deformation mechanisms: a reduction in CoF with an increase in Gr layers which increases significantly, on the other hand, when the Gr layers tear upon scratching (9).

In the current study, Cu-Gr composite foils were shear processed using a tribometer. Effects of shear forces imparted to the Cu-Gr composite at room temperature conditions on microstructure evolution were determined using different imaging and characterization techniques. Features of interest for this study included the topology of deformed 2D Gr in 3D Cu and their morphology evolution due to shear processing; and the nature of interfaces developed between Cu and Gr post shear deformation. All these features have a significant effect on composite performance and are the focus of the present study.

2.0 Materials and Methods

2.1 Materials

Gr coated Cu specimens procured from Graphenea, Spain and Grolltex, US were used in this study. The samples referred to as monolayer Cu-Gr were in the form of foils with the C11000 Cu thickness of 20 – 25 μm coated with monoatomic layer thick Gr via chemical vapor deposition (CVD). Samples referred to as trilayer comprised also of C11000 Cu foils of similar thickness that were first coated with a monoatomic layer of Gr via CVD following which two additional monoatomic layers were transferred over them mechanically. It has to be noted that there are no bonding functional groups between either the Cu and Gr species or between the individual Gr layers in the trilayer samples as specified by the supplier.

2.2 Shear Processing and Microstructural Characterization

The monolayer and trilayer Cu-Gr samples were subjected to shear deformation in dry air at room temperature using an Anton Paar pin-on-disk tribometer. A 6 mm diameter silicon nitride (Si_3N_4) sphere was used in reciprocating mode for 50 cycles, with a stroke length of 6 mm with a load of 1 N and at a sliding speed of 1 mm/s.

The microstructure of the as-received CVD Cu-Gr coupons was characterized using scanning electron microscopy (SEM) backscattered electron imaging. The microstructures of the undeformed and shear-deformed regions were characterized using SEM, transmission, and scanning transmission electron microscopy (TEM and STEM), and atom probe tomography (APT). The SEM imaging and sample preparation for S/TEM and APT (using the focused-ion beam (FIB) lift-out technique) was performed using a Thermo Fisher Scientific Quanta 200 FIB-SEM outfitted with an Oxford Instruments X-ray EDS system for compositional analysis. An FEI Titan 80–300 operated at 300 kV and an aberration, probe corrected, JEOL ARM200F operated at 200 kV were used for S/TEM. A CAMECA LEAP 4000X HR APT was used in pulsed voltage mode at a 200 KHz pulse frequency with 20% pulse fraction, a specimen temperature of 50–60 K, and a detection rate that was maintained at 0.005 atoms/pulse.

Tip-enhanced Raman spectroscopy (TERS) enables chemical imaging with few nanometer spatial resolution (11). The TERS experimental procedure is described elsewhere in detail (11). Briefly, 150 μW of P-polarized 532 nm laser light was focused onto the AFM tip apex using a 100 \times /NA = 0.7 air objective. The tip is brought into contact with the sample surface, and the enhanced local optical fields at the tip apex yield dramatically enhanced Raman scattering from the sample surface. TERS measurements were performed using silicon AFM tips (ATEC-NC) coated with 100 nm of silver. The signal was collected using a CCD camera (Andor, Newton EMCCD) coupled to a spectrometer (Andor, Shamrock 500) equipped with a 300 l/mm grating blazed at 550 nm.

3.0 Results & Discussion

3.1 Tribological Behavior of Cu-Gr Composites

The strain free back scattered SEM image of monolayer Gr deposited on C11000 foil obtained commercially is shown in Figure 1a. Local Gr wrinkles and added layers are observed in Figure 1a, which can be attributed to thermal expansion difference between the Gr and Cu as shown in higher magnification in Figure 1b. It is also possible that the add-layers occur due to the additional growth of graphene at the interface if the chemical vapor deposition process conditions were not controlled locally (12, 13). Figure 1c and 1d show the Raman spectra of the monolayer and trilayer Gr specimens. The characteristic bands of graphene are observed at 1350 cm^{-1} (D-band), 1590 cm^{-1} (G-band), and 2710 cm^{-1} (2D-band) for both the samples. The Raman spectrum of monolayer graphene is characterized by a sharp 2D peak with high intensity and a second order peak of D-band (Figure 1c) confirming the monolayer behavior. The 2D peaks of the trilayer specimen is comparatively less sharp and lower in intensity as anticipated for multilayered graphene (Figure 1d).

Figures 1e-f display the coefficient of friction (CoF) as a function of the sliding time obtained from the tribometer test conducted at room temperature. Interestingly, the trilayer coupons attained steady state and demonstrated lower CoF at an earlier time when compared to the monolayer sample. Figure 1f, represents the high resolved image of the CoF Vs time stamp on mono and tri-layer Cu-Gr coupons. The CoF rapidly increased from 0.1 to 0.2 (at 24 sec) for the monolayer sample, and from 0.1 to 0.17 (at 42 sec) for the trilayer sample. This rapid change in CoF can be attributed to rupture of the corresponding Gr layers. The increase in CoF can also be attributed to the abrasion wear on the surface. As seen from the Figure 1f, the trilayer sample had a delayed point of rupture than the monolayer resulting in higher durability of the coupon. It was also observed that the predominant wear mechanism was abrasive in nature along with partial adhesive wear with discontinuous dark patches. This indicated smearing of Gr into Cu (wear track marked with white dotted line as shown in the Figure 1g). It was noted that the EDS showed no sign of oxygen enrichment. High resolution image of the trail edge of the wear track (Figure 1h) shows that the Gr layer is lubricious; during processing, it moved away from the wear track indicating that the state of stress on the edges of the wear track was pure tensile in nature.

The presence of abrasive micro grooving with discontinuous dark patches indicating mating of Gr on the scratch surface is shown in Figure 2a and FIB lift out was done on the specific region on interest. Figure 2(b₁-b₃) show inverse pole figures in the x, y, and z directions (IPF _{x,y, &z}) and the kernel average misorientation (KAM) map from the same region as shown in Figure 2c, respectively. A deformation induced substructure can be observed with elongated Cu grains beneath the wear track. A relatively small portion on the top region of the wear track show recrystallization of grains with formation of high angle boundaries. A higher magnification SEM-BSE image of white region (from Figure 2(b₃)) is shown in Figure 2d. It was observed that the top severely deformed region has nanocrystalline Cu grains. Below this severely deformed region (extending to 1 μm below from the top), the KAM map highlights the formation of low angle misorientation boundaries extending to 3 μm from the top.

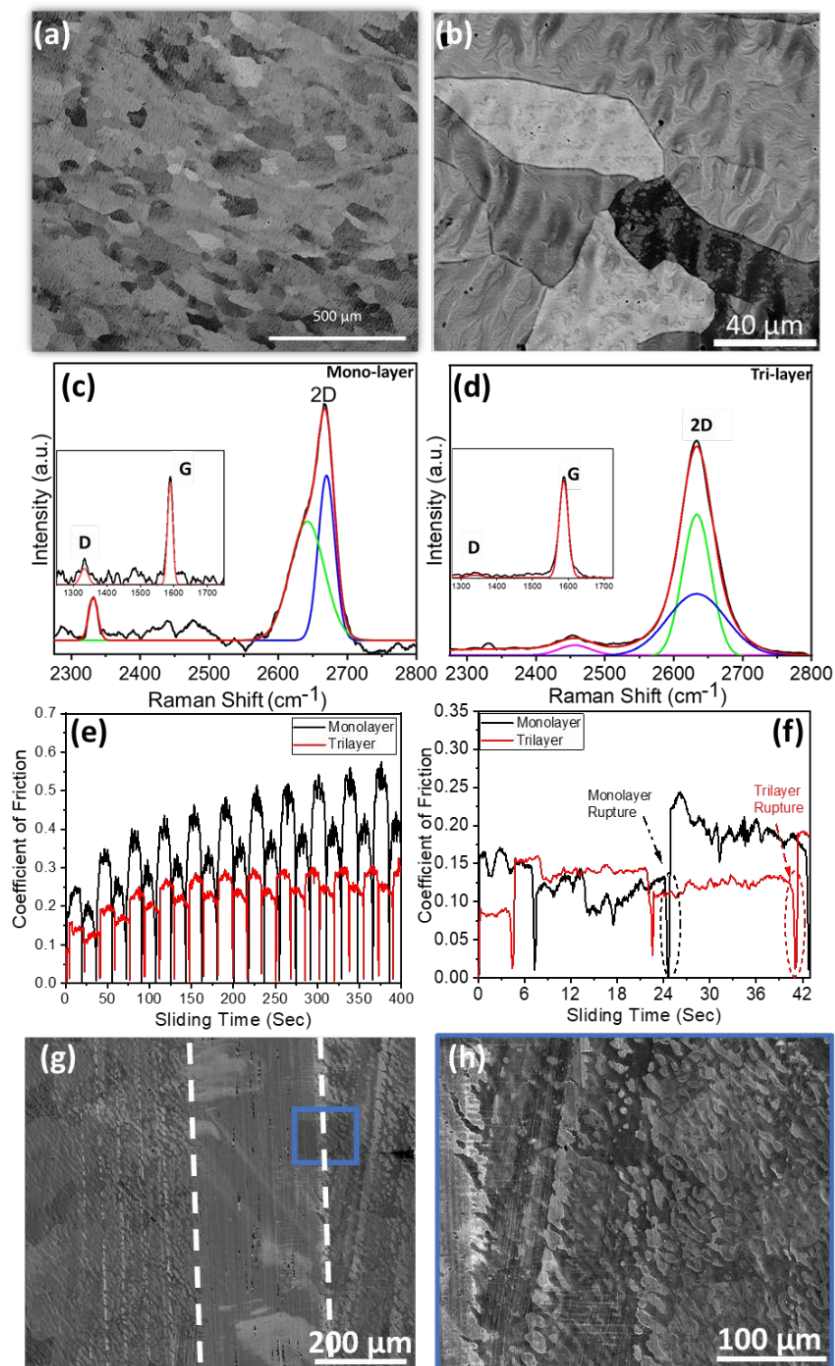


Figure 1: (a) Low magnification back scattered SEM image of Cu-Gr monolayer coupon; (b) High magnification of Cu-Gr monolayer showing added layers of graphene on the Cu-foil; (c, d) Raman spectra of Cu-Gr mono and tri-layers; (e) coefficient of friction (CoF) vs sliding time (sec) of mono and tri-layer Gr on Cu-foil slid at 1 N at 1 mm/s; (f) High resolved CoF vs sliding time (s) of mono and tri-layer Gr showing the rupture of graphene layer upon sliding; (g) wear track of tri-layer showing abrasive wear with discontinuous graphene patches; (h) Trail end edges of the wear track showing the graphene layer moving away from the wear track indicating the tensile stress acting on the sample.

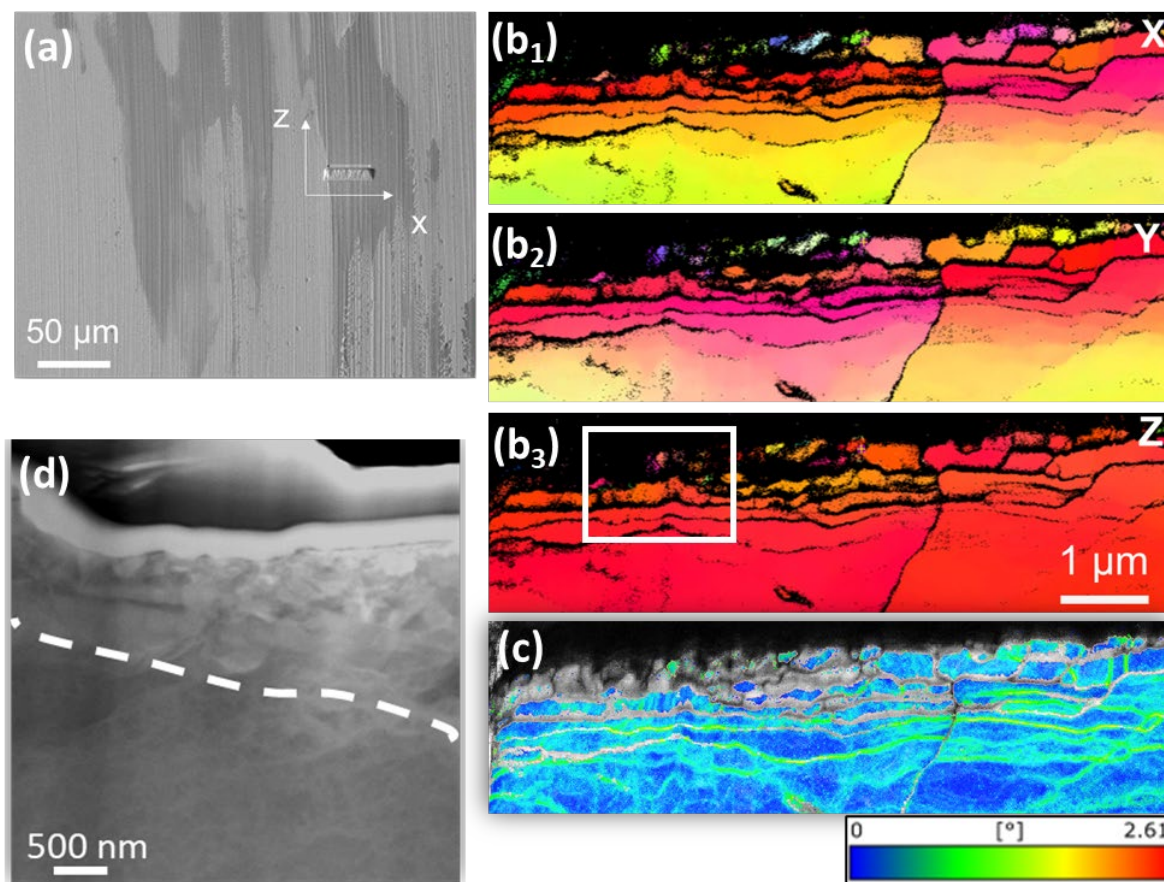


Figure 2: (a) FIB lift out of the sheared region of the Cu foil with a monolayer Gr (dark patch) where Gr is deformed on the surface (b₁-b₃) showing the grain refinement and IPF_(x, y, & z) images of the FIB lift out; (c) KAM maps of the FIB lift out; and (d) Higher magnification of the lift out showing Cu nanocrystalline region.

3.2 Composition of Sheared Cu-Gr Composites

Figure 3 shows the results from APT of the shear regime of the monolayer Cu-Gr coupon. Cu and C maps were also provided to understand the partitioning of the elements amongst the deformed regions. Figure 3a represents a three-dimensional (3D) reconstruction of the APT data of Cu and C ion map showing the Cu rich region atoms (orange dots) and C rich region (brown colored dots) smeared and segregated into Cu regions. The C ion map in Figure 3b indicates that the Gr layer had sheared into the substrate and formed clusters of C in the matrix. This shows that the applied shear forces lead to the fracture of Gr. To understand the spatial distribution of Cu and C, 2D concentration maps were plotted using the reconstruction APT data, as shown in Figure 3c and 3d. It was observed from Figure 3c that the Cu heat map showed a uniform distribution throughout the tip, whereas the carbon segregation seems to be discontinuous and more concentrated on the top (Figure 3d). The proxigram constructed from a certain area of the tip reveals the preferential partition of Cu to the matrix and C to the precipitates/ segregation, as shown in Figure 3e. Results also show significant oxygen (O) enrichment. It has to be noted that the precursor foils were processed to remove any residual O containing species such as copper oxide (CuO) from the foil surface prior to CVD. All CVD was performed in controlled environment devoid of O. Thus, it is interesting to find ~10% of O in the APT results.

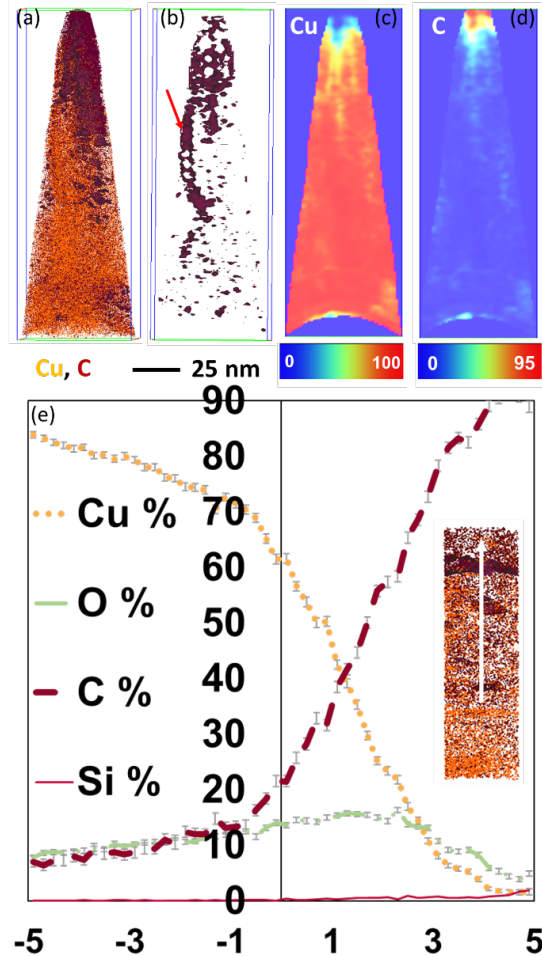


Figure 3: (a) A 3-D reconstruction showing the presence of Cu and C indicating the matrix by Cu atoms (orange) and carbon rich regions in (b) with brown atoms; (c, d) The 2-D compositional plots of Cu and C; (e) Proximity histogram of the constituent elements showing elemental partitioning across various regions.

3.3 Nanostructures in Shear Processed Cu-Gr Composites

The bright field transmission electron microscopy (BFTEM) image of the shear-deformed region of Cu depicting the grain structure and dislocation distribution inside the grains is given in Figure 4a. Note that the top layer of the shear region has ultrafine nanocrystalline grain (Figure 4b). Figure 4(c₁-c₄) show the corresponding EDS maps of Figure 4b. It was observed that the nanocrystalline grains were rich in Cu. Some of the discontinuous dark patches were seen to be partially rich in carbon indicating the Gr layer had smeared into the copper substrate upon sliding.

To investigate the sheared region in detail, high resolution TEM was used to image regions of interest marked in Figure 5a highlighted using red colored rectangular boxes. The lattice fringes seen in Figure 5b, which are almost 60 nm below the top surface (as indicated by red dotted rectangle in Figure 5a) mark the graphitic domain clusters of the size ~3 nm in the Cu matrix. The clusters have been referred to as graphitic and not Gr in this instance owing to their multi-layered nature. Figure 5d shows the TERS of the sheared region of the Cu-Gr sample. It was observed

that the G peak moved from 1590 to 1570 cm^{-1} and the ratio of the intensity of D peak to that of the G peak ($I(D)/I(G)$) is ~ 0.98 . This can be attributed to the graphite in the third stage model in which the trajectory is moving from the nanocrystalline graphite region to amorphous carbon but is not completely amorphous. On the other hand, should the G peak decrease from 1600 to 1510 cm^{-1} and the $I(D)/I(G)$ ratio approach 0 (14), the sample is identified to be more Gr in nature with increasing crystallinity. However, since the $I(D)/I(G)$ ratio for the graphitic domain in shear processed Cu-Gr composites is much greater, it is possible that the Gr in the sheared region is between nanocrystalline and amorphous structures. On the other hand, Figure 3c₄ also shows significant oxygen enrichment in the shear processed Cu-Gr composite. This is also confirmed by the APT results discussed previously. The existence of oxygen signals its presence possibly as functional groups associated with the edges of the newly formed Gr-like flakes. It is known that the presence of functional groups on Gr can also increase its defect density, increase the $I(D)/I(G)$ ratio and lead to Raman spectroscopy as seen in Figure 5d. Further analysis using X-ray photon spectroscopy, solid state nuclear magnetic resonance and X-ray diffraction may be necessary to further resolve the state of the graphitic forms, which is beyond the scope of the current study and will be a part of the future work.

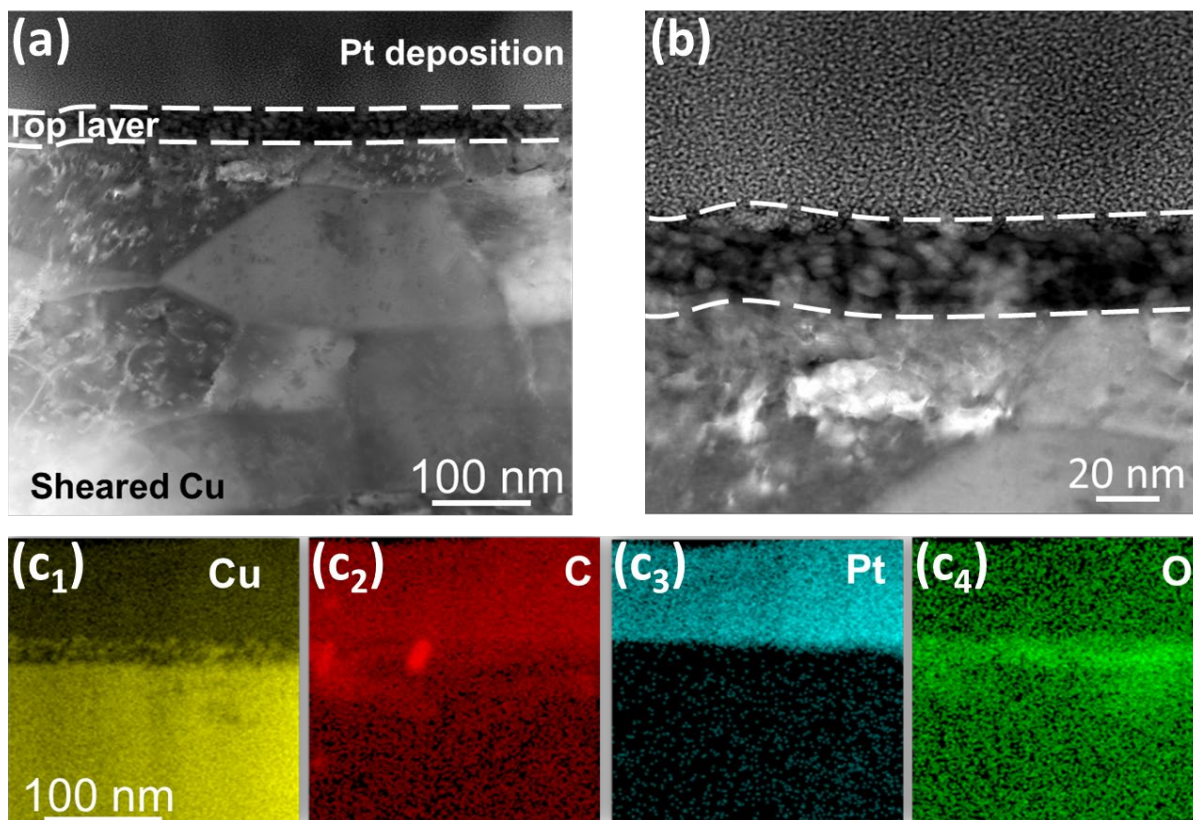


Figure 4. TEM image showing various regions of the subsurface of the wear track; (b) TEM image of the top layer indicating the nano crystalline region of the sheared region; (c₁-c₄) Corresponding EDS maps of the various constituent elements resulting nanocrystalline of copper grains and partial rich in carbon

These novel findings indicate that shear processing of Cu-Gr composites can enable the embedding of Gr in the Cu matrix where the deformed Gr need not exist exclusively at grain boundaries as previously anticipated. Figure 5c, shows the high-resolution TEM image of the interface of Cu/graphite domain which is the from top-most layer of the deformed of Figure 4a

(shown in red bold rectangle). It is observed that there is a shear strain induced bonding on Cu/graphite interface in that Cu. There is coherency between the Cu and the graphitic regions as seen in Figure 5c. Additionally, the Cu lattice is observed to be highly strained near the interface to maintain the coherency with the graphitic structure. These are the first instances of coherency demonstration between Cu and carbon regions in shear processed Cu-Gr composite to the best of the authors' knowledge. Coherency is an important finding in understanding property evolution in shear processed Cu-Gr composites; for example, a coherent microstructure indicates low carrier scattering and high electron velocities in the composite that can lead to high electrical and thermal performance.

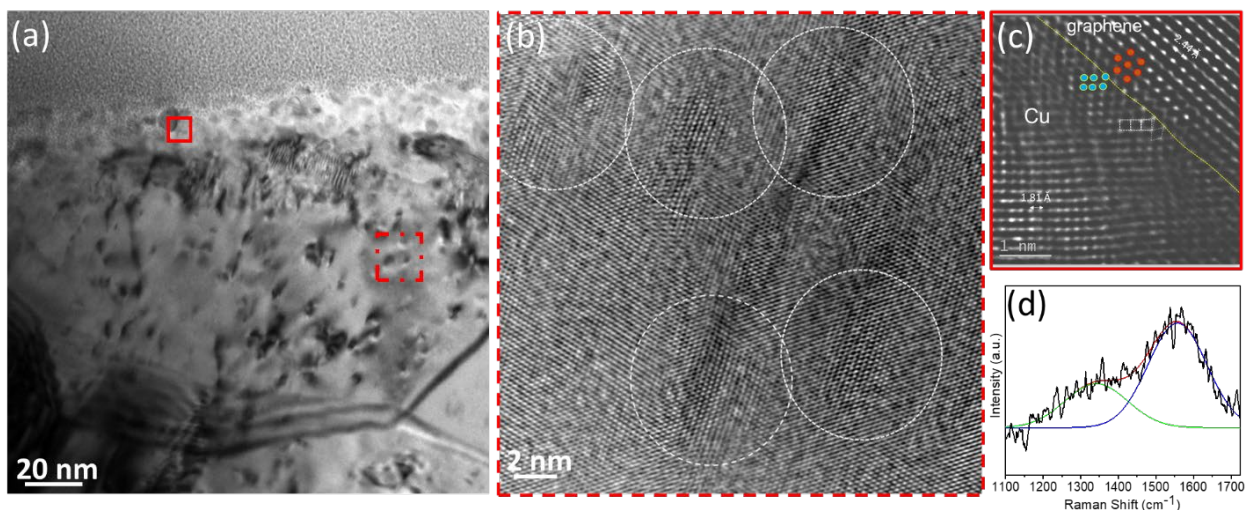


Figure 5. TEM image showing the various contrast in the initial layers of the sheared regions; (b) High resolution TEM image below ~ 60 nm of the tack showing nano domains of the graphitic clusters; (c) High resolution TEM image of the Cu/graphite interface showing bonding between Cu and graphite domains though with larger lattice misfit; (d) TERS the presence of G and D peaks corresponding to the stage between 1 and 2 where it has both nanocrystalline and amorphous graphite domains.

Another novel finding in these results is the presence of graphitic forms. Given that we started with Gr that is monolayer or trilayer thick, the results indicate that shear forces not only delaminate graphite to form Gr-like flakes; the converse is also true in that shear forces can cause monolayer or trilayer Gr foils to fracture and then agglomerate into graphitic forms. The transformation from the 2D film to an ordered 3D graphitic form observed in Figure 5b is yet to be clearly understood and may necessitate in situ deformation and imaging studies.

4.0 Conclusions

This report collates the shear deformation conditions applied on graphene coated copper foils and the resultant microstructural evolution. Tribometer experiments were performed on copper-graphene composite films with a layered structure where the number of graphene layers were varied as monolayer or trilayer. The experimental conditions were designed to observe graphene deformation and fracturing. Multimodal ex-situ characterization of the processed composites was performed to identify the copper and graphene morphology post shear deformation, chemical composition of the processed region and the nature of the copper-graphene interfaces.

During processing, both the monolayer and trilayer samples showed a sharp increase in coefficient of friction providing evidence of graphene fracture. SEM was used to observe that the copper attained an ultra-fine grain size of about ~200 nm after shear deformation compared to the precursor foil grain average size of 50 – 100 μm . The graphene was seen to fracture into individual 'flakes' about 10 – 50 μm wide and monoatomic thick. The flakes moved away from the shear zone towards the edge of the wear pathways. TEM imaging showed that the graphene may have agglomerated into graphitic forms observed inside a copper grain rather than at the grain boundaries as expected. The nature of the graphitic form needs more analysis to be understood completely. APT and TEM/EDS confirmed oxygen enrichment in the shear processed zone. The presence of oxygen, on the other hand, alludes to the possibility of agglomerated graphene/graphitic forms with functionalized edges. TERS confirmed the probability of either of these outcomes from shear processing where the results showed a high defect density in the processed graphene/graphitic forms in the copper microstructure.

This study confirms that shear forces applied during solid phase processing can be high enough to fracture graphene and disperse it into the microstructure of a metal matrix such as copper to create metastable composite structures where the graphene can exist inside the copper grains and not just at the grain boundaries as expected in equilibrium structures. The study also provides understanding into the effect of high shear forces on graphene morphology. Literature shows that low shear forces can delaminate nanoscale graphite particles into graphene like flakes. High shear forces, on the other hand, can cause monolayer graphene to fracture into individual flakes that can conversely adhere to each other to form graphitic domains that are coherent with the metal matrix. At the copper/graphene interface in the processed material, the copper was highly strained to maintain coherency with the graphene/graphitic forms.

In the future, research is needed into resolving the nature of the graphitic forms developed during shear processing. Currently, it is not clearly understood if the TERS results indicate that the graphene/graphitic forms have a structure that is transitioning from nanocrystalline to amorphous, or if their edges are functionalized. Additional NMR, XPS and XRD analysis is required to resolve these questions. Furthermore, to fully understand the evolution of copper-graphene composite microstructure under shear processing conditions, it is essential to perform similar experiments at elevated temperatures. It would also be interesting to subject the sheared samples from the current study to heat treatments to see the effects of sequential application of mechanical and thermal forces.

References

1. J. Zhao, Y. Peng, Q. Zhou, K. Zou, The current-carrying tribological properties of Cu/Graphene composites. *Journal of Tribology* **143**, 102101 (2021).
2. Z. Wang *et al.*, Ultrahigh Conductive Copper/Large Flake Size Graphene Heterostructure Thin-Film with Remarkable Electromagnetic Interference Shielding Effectiveness. *Small* **14**, 1704332 (2018).
3. J.-f. Li, L. Zhang, J.-k. Xiao, K.-c. Zhou, Sliding wear behavior of copper-based composites reinforced with graphene nanosheets and graphite. *Transactions of Nonferrous Metals Society of China* **25**, 3354-3362 (2015).
4. Y. Meng, F. Su, Y. Chen, Synthesis of nano-Cu/graphene oxide composites by supercritical CO₂-assisted deposition as a novel material for reducing friction and wear. *Chemical Engineering Journal* **281**, 11-19 (2015).
5. P. Hidalgo-Manrique *et al.*, Copper/graphene composites: a review. *Journal of materials science* **54**, 12236-12289 (2019).
6. B. Vasić, A. Zurutuza, R. Gajić, Spatial variation of wear and electrical properties across wrinkles in chemical vapour deposition graphene. *Carbon* **102**, 304-310 (2016).
7. Y. Huang *et al.*, Wear evolution of monolayer graphene at the macroscale. *Carbon* **115**, 600-607 (2017).
8. M.-S. Won, O. V. Penkov, D.-E. Kim, Durability and degradation mechanism of graphene coatings deposited on Cu substrates under dry contact sliding. *Carbon* **54**, 472-481 (2013).
9. W. Wang, Q. Peng, Y. Dai, Z. Qian, S. Liu, Distinctive nanofriction of graphene coated copper foil. *Computational Materials Science* **117**, 406-411 (2016).
10. A. Zambudio *et al.*, Fine defect engineering of graphene friction. *Carbon* **182**, 735-741 (2021).
11. C.-F. Wang, B. T. O'Callahan, D. Kurouski, A. Krayev, P. Z. El-Khoury, The prevalence of anions at plasmonic nanojunctions: A closer look at p-nitrothiophenol. *The journal of physical chemistry letters* **11**, 3809-3814 (2020).
12. N. Liu *et al.*, The origin of wrinkles on transferred graphene. *Nano Research* **4**, 996 (2011).
13. Q. Li *et al.*, Growth of adlayer graphene on Cu studied by carbon isotope labeling. *Nano letters* **13**, 486-490 (2013).
14. A. C. Ferrari, J. Robertson, Interpretation of Raman spectra of disordered and amorphous carbon. *Physical review B* **61**, 14095 (2000).

Pacific Northwest National Laboratory

902 Battelle Boulevard
P.O. Box 999
Richland, WA 99354
1-888-375-PNNL (7665)

www.pnnl.gov